# Femtosecond and nanosecond laser fabricated substrate for surface-enhanced Raman scattering

**Adam Hamdorf,[1] Matthew Olson,[1] Cheng-Hsiang Lin,[1] Lan Jiang,[2] Jun Zhou,[3] Hai Xiao,[4] and Hai-Lung Tsai[1,*]**

[1]*Department of Mechanical and Aerospace Engineering, Missouri University of Science and Technology, Rolla, Missouri 65409, USA*

[2]*School of Mechanical Engineering, Beijing Institute of Technology, Beijing 100081, China*

[3]*Department of Mechanical Engineering, The Pennsylvania State University Erie, Pennsylvania 16563, USA*

[4]*Department of Electrical and Computer Engineering, Missouri University of Science and Technology, Rolla, Missouri 65409, USA*

**Corresponding author: tsai@mst.edu*

Received May 31, 2011; revised July 15, 2011; accepted July 15, 2011;
posted August 3, 2011 (Doc. ID 148525); published August 22, 2011

We report a simple and repeatable method for fabricating a large-area substrate for surface-enhanced Raman scattering. The substrate was processed by three steps: (i) femtosecond (fs) laser micromachining and roughening, (ii) thin-film coating, and (iii) nanosecond laser heating and melting. Numerous gold nanoparticles of various sizes were created on the surface of the silicon substrate. The 3D micro-/nanostructures generated by the fs laser provide greater surface areas with more nanoparticles leading to 2 orders of magnitude higher of the enhancement factor than in the case of a flat substrate. Using an He–Ne laser with a 632.8 nm excitation wavelength, the surface-enhanced Raman scattering enhancement factor for Rhodamine 6G was measured up to $2 \times 10^7$. 

*OCIS codes:* 300.6450, 240.6695.

The phenomenon of surface-enhanced Raman scattering (SERS) was first observed over 35 years ago [1,2]. Since its discovery, SERS has interested researchers because of its ability to identify specimen information [3,4] with enough sensitivity to be capable of single molecular detection [5]. While SERS has shown enormous potential, one of its intrinsic drawbacks is the limited materials capable of providing high enhancement factors (EFs). Substrates have primarily utilized the noble metals in the format of nanoparticles such as silver and gold and occasionally copper to achieve sufficient enhancements due to their superior optical properties [6]. The selection of the material depends on the application: while silver provides the highest EFs, gold has higher chemical stability in air.

Because the EF of the signal depends on the substrate's ability to generate surface plasmon resonance [7], much research has focused on different methods for positioning nanoparticles in ways conducive to generating strong signals. Creating patterned surface structures with a femtosecond (fs) laser has yielded high EFs when used in conjunction with methods such as lithography [8] or chemical plating [9]. Laser machining in silver nitrate solutions [10] or on Ag-doped materials [11] has also produced exceptional EFs due to the nanostructures formed by the laser processing.

In this study, fabrication of the SERS substrate was first carried out with an fs laser to generate micro- and nanoscale surface features. All silicon wafers were cleaned before and after fs laser machining in an ultrasonic bath with a 70% ethanol solution for 10 min and were then rinsed with distilled water. The fs laser (Legen-F, Coherent, Inc.) had a central wavelength, maximum repetition rate, and laser pulse width of 800 nm, 1 kHz, and 120 fs, respectively. The output power for the laser was reduced through the combination of a half-wave plate and linear polarizer. The laser beam was focused with an objective lens (Olympus UMPLFL 10×, NA = 0.3) onto the silicon substrate mounted on a five-axis motion stage (Aerotech) with a resolution of about 1 $\mu$m. The fs laser spot size was approximately 4 $\mu$m.

Low-pressure air was applied to the substrate during fabrication to minimize the silicon spatter redepositing on the machined area. Trenches were created on the silicon surface by using a 72 $\mu$W laser power, a 1 kHz repetition rate, and a scan speed of 5 mm/ min. Horizontal line scans were 5 mm long, and each was vertically spaced 2 $\mu$m from one another so there was a 50% overlap between the rows due to the 4 $\mu$m laser spot size. A total of 30 line scans were made on the surface, resulting in periodic trenches over a 5000 $\mu$m × 60 $\mu$m area on the silicon surface, as shown in Fig. 1, which is consistent with previously reported results [12]. In Fig. 1, the width of the "stripe" is approximately 406 nm, the center-to-center distance between two stripes is 571 nm, the "gap" between two strips is 165 nm, and the depth of the trench is 3 $\mu$m.

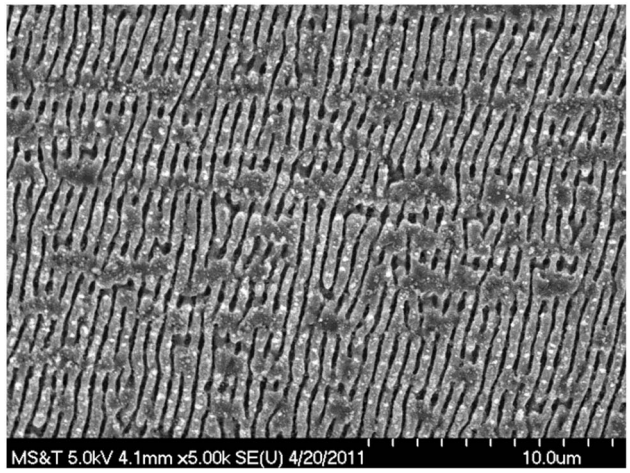


Fig. 1. Scanning electron microscope (SEM) image of the silicon substrate after fs laser machining.

 

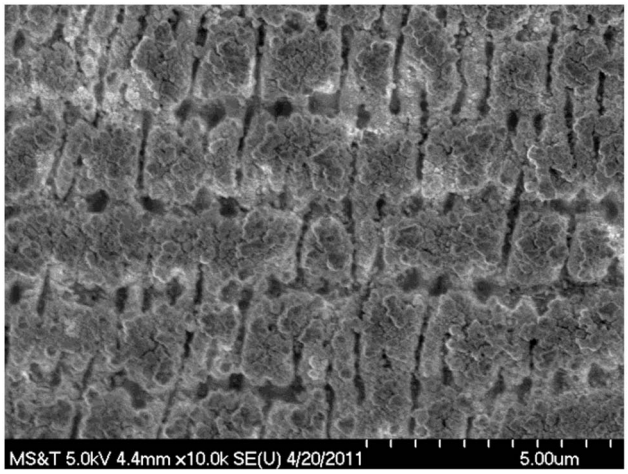


Fig. 2. SEM image of the silicon substrate topography after fs laser machining and gold coating.


Fig. 3. SEM image of the silicon substrate after fs laser machining, gold coating, and ns laser melting.

A 50 nm thick gold film was coated on the fs laser machined substrate using a sputter coater (Desk V, Denton Vacuum). The vacuum of the sputter coater was brought down to 40 mTorr before starting the argon sputtering gas. A low target current of 8 mA was used to coat the substrates for a total of 7 min. As shown in Fig. 2, the gold films cannot cover the trenches, and they are not smooth and continuous. This can be attributed to the large trenches in the middle of the silicon bridges, which is different than sputtering on a flat surface, where the gold will distribute evenly and will have nanoscale breaks and islands [13].

The final step in the substrate processing was laser heating and melting of the gold film using a nanosecond (ns) laser micromachining system that consisted of a frequency-tripled Nd:YAG laser (AVIA 355-X, Coherent) and a computer-controlled four-axis motion stage (Aerotech). The central wavelength, maximum repetition rate, and pulse width of the ns laser were 355 nm, 200 kHz, and 30 ns, respectively. If the ns laser intensity is too high, the gold film can be ablated and removed. Likewise, if the ns laser intensity is too low, the gold film may not be melted to become nanoparticles. Hence, the ns laser energy was adjusted until nanoparticles were generated with the following laser parameters: 2000 Hz of repetition rate, 4 mm/ min of scanning speed, and 120 $mJ/cm^2$ of fluence. Note that it is not the purpose of this study to optimize the laser parameters to generate the maximum possible nanoparticles on the substrate.

Previous research has shown that a flat gold coating will form gold nanoparticles when treated with an ns laser [13]. In contrast, as shown in Fig. 3, the defocused ns laser has generated a wider range of nanoparticle sizes, which range from 10 to 200 nm. However, approximately more than 80% of the nanoparticles are in the range of 20 to 50 nm in diameter. The 3D micro-/ nanostructures provide larger surface areas and more nanoparticles on the surface of the substrate. In addition, the 3D structures may help with concentrating and trapping the light on the nanoparticles, leading to higher EFs.

SERS was then tested on the different areas of the substrate. All substrates were incubated in Rhodamine 6G (R6G) solutions for 1 h at room temperature. This provided a consistent distribution of the R6G on the entire substrate surface. The SERS signal was measured with a commercial Ramanscope (Jobin Yvon) using an He–Ne laser with a 632.8 nm wavelength as the excitation source, and the measuring laser spot size was about 10 $\mu$m. The grating and objective lens used were 600 line/mm and 10× (NA = 0.25), respectively. A concentration of $10^{-3}$ M was used for the normal Raman substrate and $10^{-6}$ M for all other substrates. The accumulation time and the intensity of the He–Ne laser were varied. All SERS-active substrates used a 5 s acquisition time and an intensity of 1.7 mW, except the fs laser machined, gold-coated, ns laser heated area, which used power of 1.7 $\mu$W. The uncoated substrates used acquisition times of 3 and 4 s for the machined and unmachined areas, respectively, with laser power of 17 mW.

Because the fs laser affected the topography of the substrate, it also changed the Raman spectrum. The SERS spectrum from sputtering on a flat surface [14] or by ns laser melting a flat gold coating [13] has already been discussed previously. A good-quality spectrum is also obtained by gold coating and melting over an fs laser machined area, as shown in Fig. 4(a). Distinct Raman peaks were produced with narrow linewidths for low excitation powers. Figure 4(b) shows the spectrum for the fs laser-machined, gold-coated area, which produced a comparable signal to Fig. 4(a) but used 1000 times the excitation power. There were not visible Raman peaks when acquiring the signal on the machined-only area, as shown in Fig. 4(c).

The EF was calculated with the following equation:

$$\mathrm{EF} = \frac{I_{\mathrm{SERS}} \times N_{\mathrm{NR}}}{I_{\mathrm{NR}} \times N_{\mathrm{SERS}}}, \tag{1}$$

where $I$ and $N$ represent the intensity and number of molecules probed, respectively, and the subscripts SERS and NR denote the acquisition from either the SERS-active substrate or the normal Raman control substrate. The SERS signal EFs are shown in Table 1. The columns in Table 1 indicate the order and type of substrate processing, where Au, NS, and FS indicate gold coating, ns laser melting, and fs laser machining, respectively. Note that in the cases of Au and Au + NS, the normal Raman

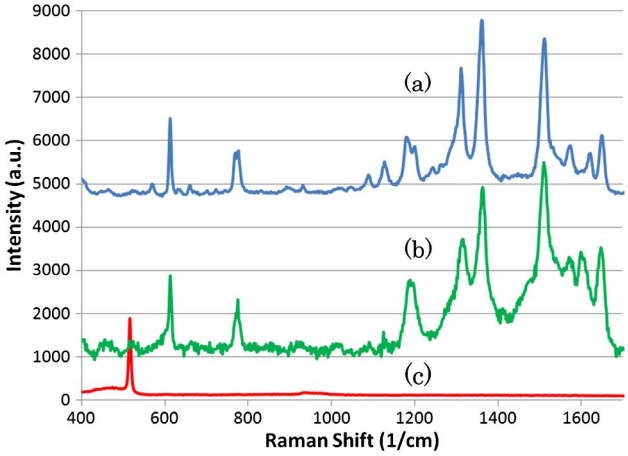


Fig. 4. (Color online) SERS spectrum for (a) fs laser-machined, gold-coated, ns laser treated area with $10^{-6}$ M R6G, 1.7 $\mu$W laser power, and 5 s acquisition time; (b) fs laser-machined and gold-coated substrate with $10^{-6}$ M R6G, 1.7 mW laser power, and 5 s acquisition time; and (c) fs laser-machined silicon with $10^{-3}$ M R6G, 17 mW laser power, and 3 s acquisition time.

and SERS substrates are flat bare silicon, while in the cases of FS + Au and FS + Au + NS, the normal Raman and SERS substrates are machined by an fs laser. Therefore, the surface roughness of the normal Raman and SERS substrates is close to each other. It is reasonable to assume that the measured molecules on normal Raman and SERS are identical, and the EF can be simplified to the ratio of intensity of SERS and normal Raman. The EFs given in Table 1 are the averaged values for five substrate samples, and each was measured at 10 different locations. The variations of the data from the averaged values are estimated to be in the range of $\pm 30\%$ for all cases. It has been observed before that just sputter coating alone could produce SERS [14], and the results agree with these findings. The same was true for the ns melting; while it was known that this method could produce SERS signals [13], it was necessary to find the EFs again in this Letter for comparison purposes. Coating gold over the fs machined area produced the lowest EFs. However, ns annealing the fs laser grid area achieved EFs of up to $10^7$, much higher than all of the other SERS-active areas.

In summary, the SERS EFs up to $10^7$ were achieved by combining fs laser machining, gold coating, and ns laser melting. The proposed process is simple and repeatable, which can increase the EFs 2 orders of magnitude as compared to the previous proposed method with a flat substrate. The 3D micro-/nanostructures can increase surface areas and the number of gold nanoparticles with different sizes leading to the higher EFs.

**Table 1. Enhancement Factors for SERS-Active Regions**

| Raman Shift | Au | Au, NS | FS, Au | FS, Au, NS |
|---|---|---|---|---|
| 610 | $3.6E+04$ | $1.8E+05$ | $8.1E+03$ | $8.7E+06$ |
| 1310 | $4.7E+04$ | $2.3E+05$ | $1.4E+04$ | $1.6E+07$ |
| 1363 | $6.6E+04$ | $2.7E+05$ | $1.8E+04$ | $2.0E+07$ |
| 1509 | $6.4E+04$ | $2.5E+05$ | $2.2E+04$ | $1.9E+07$ |

This work was supported by the U.S. Department of Energy (DOE) under contract DE-FE0001127 and by the National Natural Science Foundation of China (NSFC) under grants 90923039 and 50705009.

## References

1. M. Fleischmann, P. J. Hendra, and A. J. McQuillan, Chem. Phys. Lett. **26**, 163 (1974).
2. D. J. Jeanmaire and R. P. Van Duyne, J. Electroanal. Chem. **84**, 1 (1977).
3. H. Chon, C. Lim, S. M. Ha, Y. Ahn, E. K. Lee, S. I. Chang, G. H. Seong, and J. Choo, Anal. Chem. **82**, 5290 (2010).
4. Y. S. Huh, A. J. Chung, and D. Erickson, Microfluid. Nanofluid. **6**, 285 (2009).
5. S. Nie and S. R. Emory, Science **275**, 1102 (1997).
6. M. Kerker, J. Opt. Soc. Am. B **2**, 1327 (1985).
7. M. Moskovits, J. Raman Spectrosc. **36**, 485 (2005).
8. E. Diebold, P. Peng, and E. Mazur, J. Am. Chem. Soc. **131**, 16356 (2009).
9. Y. Han, X. Lan, T. Wei, H. Tsai, and H. Xiao, Appl. Phys. A **97**, 721 (2009).
10. C. H. Lin, L. Jiang, Y. H. Chai, H. Xiao, S. J. Chen, and H. L. Tsai, Opt. Express **17**, 21581 (2009).
11. Z. Zhou, J. Xu, Y. Cheng, Z. Xu, K. Sugioka, and K. Midorikawa, Jpn. J. Appl. Phys. **47**, 189 (2008).
12. J. Bonse, S. Baudach, J. Kruger, W. Kautek, and M. Lenzner, Appl. Phys. A **74**, 19 (2002).
13. C. H. Lin, L. Jian, J. Zhou, H. Xiao, S. J. Chen, and H. L. Tsai, Opt. Lett. **35**, 941 (2010).
14. L. May, C. E. Vallet, and Y. H. Lee, J. Vac. Sci. Technol. A **15**, 238 (1997).